Retinal Pigment Epithelial Features in Central Serous Chorioretinopathy Identified by Polarization-Sensitive Optical Coherence Tomography

Philipp Roberts,[1] Bernhard Baumann,[2] Jan Lammer,[1] Bianca Gerendas,[1] Julia Kroisamer,[1] Wolf Bühl,[1] Michael Pircher,[2] Christoph K. Hitzenberger,[2] Ursula Schmidt-Erfurth,[1] and Stefan Sacu[1]

[1]Department of Ophthalmology and Optometry of the Medical University of Vienna, Vienna, Austria
[2]Center for Medical Physics and Biomedical Engineering of the Medical University of Vienna, Vienna, Austria

Correspondence: Stefan Sacu, Department of Ophthalmology and Optometry of the Medical University of Vienna, Waehringer Guertel 18-20, 1090 Vienna, Austria; stefan.sacu@meduniwien.ac.at.

Submitted: October 25, 2015
Accepted: January 24, 2016

Citation: Roberts P, Baumann B, Lammer J, et al. Retinal pigment epithelial features in central serous chorioretinopathy identified by polarization-sensitive optical coherence tomography. *Invest Ophthalmol Vis Sci*. 2016;57:1595–1603. DOI:10.1167/iovs.15-18494

Purpose. To determine the subclinical RPE lesions detected by tissue selective polarization-sensitive optical coherence tomography (PS-OCT) in eyes with central serous chorioretinopathy (CSC) and to compare PS-OCT findings to current imaging standards.

Methods. In this prospective observational case series, individuals with unilateral or bilateral active CSC were imaged using PS-OCT at baseline and after resolution of serous retinal detachment. Features seen on PS-OCT were compared with corresponding lesions as seen on conventional, intensity-based spectral-domain OCT (SD-OCT), fluorescein angiography, and indocyanine green angiography (ICGA). Features of RPE evaluated by PS-OCT were as follows: area and volume of pigment epithelium detachment (PED), presence of RPE aggregations, RPE skip lesions, RPE thickening, and RPE atrophy.

Results. Twenty-five study eyes and 23 fellow eyes of 25 participants (2 women, 23 men; mean age ± standard deviation = 40.5 ± 7.4 years) were included and followed for 6.1 ± 3 months. Study eyes and fellow eyes with recurrent CSC showed more RPE abnormalities in PS-OCT than eyes with acute CSC, which correlated well with lesions in ICGA. Closure of the leakage site was observed only in eight (32%) eyes after resolution of subretinal fluid (SRF). All study eyes showed widespread RPE aggregates and 23 (92%) eyes showed RPE skip lesions after resolution of SRF.

Conclusions. Features of RPE indicative of previous episodes of CSC detected by PS-OCT correspond well to choroidal lesions in ICGA. In addition, noninvasive PS-OCT imaging enables detection of RPE microrips and aggregations invisible to clinical examination or SD-OCT, thus providing valuable information about disease processes in vivo.

Keywords: central serous chorioretinopathy, polarization-sensitive optical coherence tomography, retinal pigment epithelium

Central serous chorioretinopathy (CSC), an idiopathic disease of the posterior pole, typically affecting young and otherwise healthy persons in their third to fifth decades, is one of the most common causes of mild to moderate visual impairment. There is predominance in males with a male to female ratio between 2.7:1 and 7:1.[1–7] Central serous chorioretinopathy is characterized by serous retinal detachment and/or RPE detachment. A pressure buildup in the choroid is believed to overwhelm the physical resistance of the RPE, thus causing RPE detachment (PED) and/or microrips or "blowouts" of the RPE, leading to accumulation of subretinal fluid (SRF).[1,5,6]

Broadly, three types of CSC are differentiated: acute, recurrent and chronic types.[1,8] In acute CSC, RPE changes are mostly minor and usually localized. The term "chronic CSC" refers to cases with serous retinal detachments of 6 months or longer.[6] Chronic and recurrent cases of CSC are often associated with more severe and widespread RPE defects than seen in the acute form. The role of the RPE is still not well understood in the pathogenesis of CSC.[9,10] Using optical coherence tomography (OCT), in vivo imaging of the RPE layer and its lesions in CSC has become feasible.[10–16] However, differentiation of layers with similar reflectivity (e.g., RPE, photoreceptor layers, subretinal hyperreflective material) is difficult using intensity-based OCT technology, especially in eyes with alteration of the retinal contour and microstructure caused by retinal disease.

Polarization-sensitive OCT (PS-OCT), an extension of conventional OCT, is a new imaging modality, capable of detecting the RPE based on its polarization-scrambling properties.[17,18] Melanin granules in the RPE cells cause scrambling of the polarization state of the backscattered probing light beam. This feature can be exploited in order to segment the RPE layer.[19–24]

Purpose of this study was to evaluate the RPE for subclinical changes in eyes with CSC with episodes of neurosensory retinal detachment using PS-OCT as a novel imaging technique and to compare findings to current imaging standards.

Methods

Participants

Twenty-five consecutive participants with acute unilateral or bilateral CSC with serous retinal detachment (first episode or recurrence) were included after obtaining written informed consent. The study protocol was adherent to the tenets of the declaration of Helsinki and prospectively approved by the local ethics committee (institutional review board). Participants were followed up until resolution of SRF. Individuals aged less than 18 years; pregnant women and individuals with a history of retinal disease other than CSC; and patients with a history of previous treatment for CSC (PDT, laser, anti-VEGF, acetazolamide or eplerenone) in the eye with active CSC were not included in the study. All examinations were performed by the same retina specialist at the department of ophthalmology and optometry at the Medical University of Vienna following a standardized protocol.

Examinations

The diagnosis of CSC was based on ocular examination, SD-OCT, fluorescein angiography (FA) and indocyanine green angiography (ICGA). Follow-up visits were scheduled every 6 weeks. At every visit, best corrected visual acuity (BCVA) testing following ETDRS criteria, a comprehensive ophthalmologic examination as well as color fundus (CF) photography, SD-OCT, infrared, short wavelength autofluorescence (excitation: 488 nm; emission $>$ 500 nm), near-infrared autofluorescence (excitation: 787 nm; emission $>$ 810 nm) and red free imaging was performed. Imaging of PS-OCT was performed at baseline, after 3 months, when fluid resolved and again 3 months after resolution of SRF. If subretinal fluid did not reduce within 3 months of onset of symptoms, PDT was considered as treatment of choice and patients were excluded from the study. The same accounted for cases that required anti-VEGF treatment for choroidal neovascularizations (CNV) secondary to CSC.

Based on ICGA and FA, eyes were categorized as acute or recurrent CSC. Eyes with one or more distinct origins of dye leakage (all showing the same degree of leakage indicative of simultaneous onset) were classified as acute. Eyes with disseminated areas of different patterns of dye accumulation, indicative of previous episodes of CSC, were classified as recurrent. In two patients, where ICGA or FA imaging was not possible, the classification (acute versus recurrent) was done based on fundus autofluorescence and near-infrared imaging. For this purpose, the images were thoroughly reviewed for features (e.g., distinct areas of hypoautofluorescence, "descending tracts," areas of ill-defined hypo- and hyperautofluorescence) indicative of RPE damage due to previous episodes of CSC. These changes had to be present in a different location than the area of neuroretinal detachment caused by the acute episode of CSC.

Polarization-Sensitive OCT

The polarization-sensitive OCT device used in this study was a prototype developed and provided by the Center for Medical Physics and Biomedical Engineering, working at a center wavelength of ~840 nm with a raster scanning speed of up to 20.000 A-scans per second. Details of the PS-OCT system can be found elsewhere.[21] The system is capable of acquiring three-dimensional datasets of the size of $6.2 \times 6.7 \times 3.3$ mm (X $\times$ Y $\times$ Z) with an axial resolution of 4.5 μm in tissue, simultaneously measuring reflectivity, retardation, optic axis orientation and degree of polarization uniformity (DOPU).[21,22] The value of DOPU, calculated with the use of Stokes vector analysis of the backscattered light, is a way to quantitatively describe the polarization-scrambling (depolarizing) properties of tissue.

The segmentation of RPE is based on the fact that melanin-containing structures (i.e., RPE cells) alter the polarization state of light randomly, whereas polarization-preserving structures such as photoreceptors or birefringent structures such as the retinal nerve fiber layer backscatter light in a well-defined polarization state. Hence, the DOPU values (ranging from 0 to 1) of the different layers of the ocular fundus differ significantly, which can be exploited to differentiate these tissues based on their physical properties. Tissues that reflect light with a well-defined polarization state have DOPU values of approximately 1, whereas depolarizing tissues have DOPU values <1. For the purpose of this study, structures with a DOPU value ≤ 0.8 were classified as depolarizing.

The volume scans of PS-OCT were evaluated quantitatively for area and volume of PEDs (mm^2 and mm^3) and qualitatively for the presence of the following findings (Fig. 1):

1. RPE atrophy (absence of RPE of a well-defined area with a diameter $\geq$175 μm)
2. RPE thickening (areas of thickening of depolarizing material exceeding twice the thickness of the segmented regular RPE band)
3. RPE skip lesions (punctuate gaps in the RPE with a diameter $<$175 μm)
4. RPE aggregations (punctuate thickening of the RPE exceeding double the regular RPE height)

Both PS-OCT B-scans and en-face maps were analyzed for the parameters mentioned above by a retina expert and an optical engineer familiar with the clinical and imaging features of CSC and PS-OCT (PR, BB).

Area (mm^2) and volume (mm^3) of PEDs were calculated using customized software, details of which can be found elsewhere.[21] In brief, the RPE, segmented by its depolarizing properties, serves as the reference for the calculation of the deviation from an assumed healthy RPE position, which is calculated by an algorithm to fit the curvature of the posterior pole. Differences between the actual RPE position and the assumed healthy RPE position are calculated for every single A-scan in order to segment and quantify the area (mm^2) and volume (mm^3) of the PED.

For every eye, PED area and volume were assessed in a circle positioned closely around the PED using the algorithm described above. Pigment epithelium detachment was defined as a focal elevation of the RPE with an area of nonreflective space between the posterior boundary of the RPE and Bruch's membrane. A minimum height (distance between the actual RPE position and an assumed healthy RPE position) of 10 pixels (approximately 25 μm) was chosen as a threshold for PED analysis.

Statistics

For statistical analyses, commercial software (SPSS Statistics, version 21; IBM Corp., Armonk, NY, USA) was used.

Paired *t*-tests were performed in order to test for a significant change in PED sizes and in visual acuity in study eyes from baseline to the end of study. Independent samples Mann-Whitney *U* test and independent samples median test was used to assess significant difference in time to resolution of SRF in acute and recurrent CSC. Descriptive statistics were performed for the qualitative RPE changes. A *P* value of less than 0.05 was considered statistically significant.

Investigative Ophthalmology & Visual Science

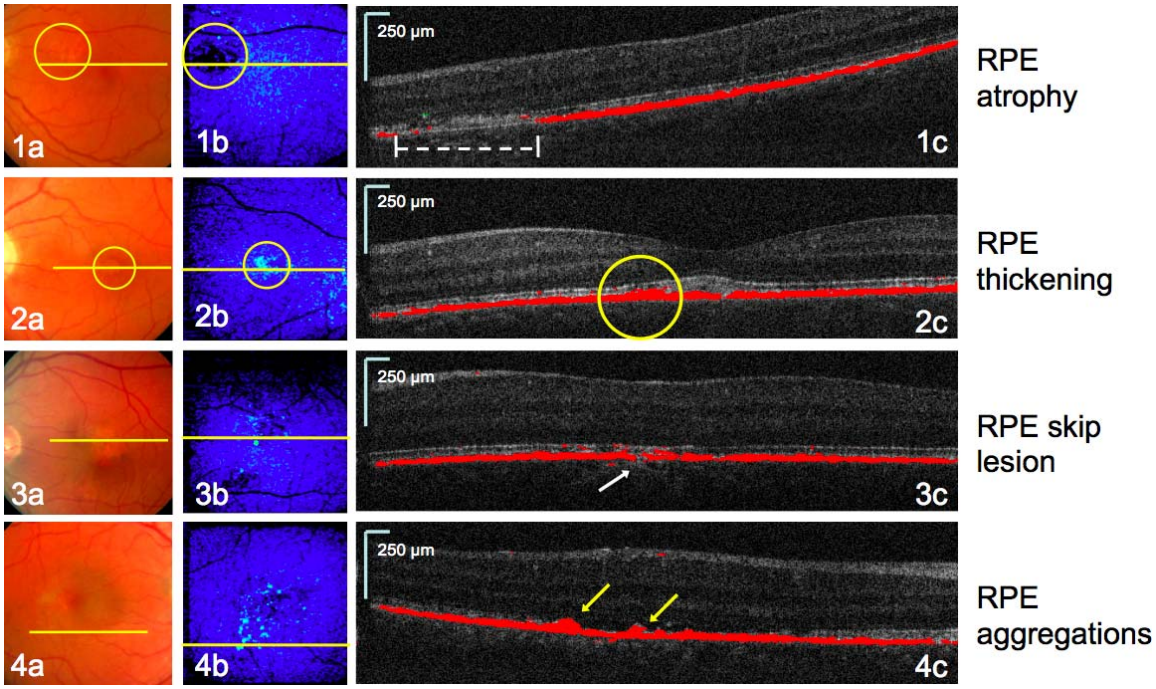

Figure 1. Features of RPE evaluated on PS-OCT. Color fundus photographs (**1a–4a**); PS-OCT RPE thickness maps (**1b–4b**); and PS-OCT RPE segmentation B-scans (**1c–4c**) corresponding to the *yellow horizontal lines* in the en-face images. Images illustrate examples of RPE atrophy ([**1a–c**], *dashed white line*); RPE thickening ([**2a–c**], *yellow circle*); RPE skip lesion ([**3a–c**], *white arrow*) and RPE aggregations ([**4a–c**]: *yellow arrows*).

Results

Forty-eight eyes (25 study eyes diagnosed with acute CSC, 23 fellow eyes) of 25 consecutive patients (2 female, 23 male) were included in this study. One fellow eye could not be imaged due to corneal scarring, one fellow eye showed severe motion artefacts and was therefore not included in the analysis. Mean ± SD age was 40.5 ± 7.4 years, ranging from 26 to 54 years. Follow-up was 6.1 ± 3.0 months. Time until resolution of SRF was 3.8 ± 2.6 months. Three patients were diagnosed with bilateral CSC (all male). One of these three affected fellow eyes had to be treated with PDT for nonresolving CSC and the two others showed early recurrence of SRF at the end of study visit and were therefore not evaluated as study eyes. Only one participant reported a previous episode of CSC in the study eye that had resolved spontaneously about 1 year prior to study entry. None of the other study participants had been diagnosed with CSC prior to study entry.

On angiography, based on previous descriptions of leakage patterns in CSC, 2 study eyes showed a smokestack leakage pattern, 10 eyes an inkblot leakage pattern, 7 eyes a diffuse leakage, and 4 eyes an undefined grade of leakage or no definite leakage.[25,26] In two patients, neither FA nor ICGA was possible. Fourteen eyes were classified as acute and 11 eyes as recurrent CSC.

A detailed description of the study population's characteristics is reported in Table 1.

Pigment Epithelium Detachment

Pigment epithelium detachments were found in 12 study eyes and in 2 fellow eyes at baseline and in 11 study eyes and 2 fellow eyes after resolution of SRF. In three eyes (all diagnosed with recurrent CSC), multiple PEDs were observed. However, in each of these eyes, only one of the PEDs showed leakage on ICGA or FA. Pigment epithelium detachments without signs of leakage were regarded as inactive and were not included in the analysis. Median PED area and volume were 0.12 mm^2 (range, 0.01–0.73 mm^2) and 0.0036 mm^3 (range, <0.0001–0.0415 mm^3) at baseline and 0.10 mm^2 (range, 0.00–0.67 mm^2) and 0.0035 mm^3 (range, 0.0000–0.0317 mm^3) after resolution of fluid. There was no statistically significant difference in PED area ($P = 0.06$) or volume ($P = 0.07$) at baseline and after resolution of SRF in our study population.

Table 1. Characteristics of Study Population

Characteristics of Study and Fellow Eyes				
	Baseline		End of Study	
Characteristics	Study Eyes, $n = 25$	Fellow Eyes, $n = 23$	Study Eyes, $n = 25$	Fellow Eyes, $n = 23$
BCVA (ETDRS letter score)	85.4 ± 6.6	91.4 ± 6.0	90 ± 5.5	91 ± 6.9
SRF present, *n* (%)	25 (100)	3 (13)	0 (0)	3 (13)
PED present, *n* (%)	12 (48)	2 (9)	11 (44)	2 (9)

Values in mean ± standard deviation or absolute numbers (no.) and percent. BCVA, best corrected visual acuity (given in ETDRS letter score). PED, pigment epithelium detachment; SRF, subretinal fluid.

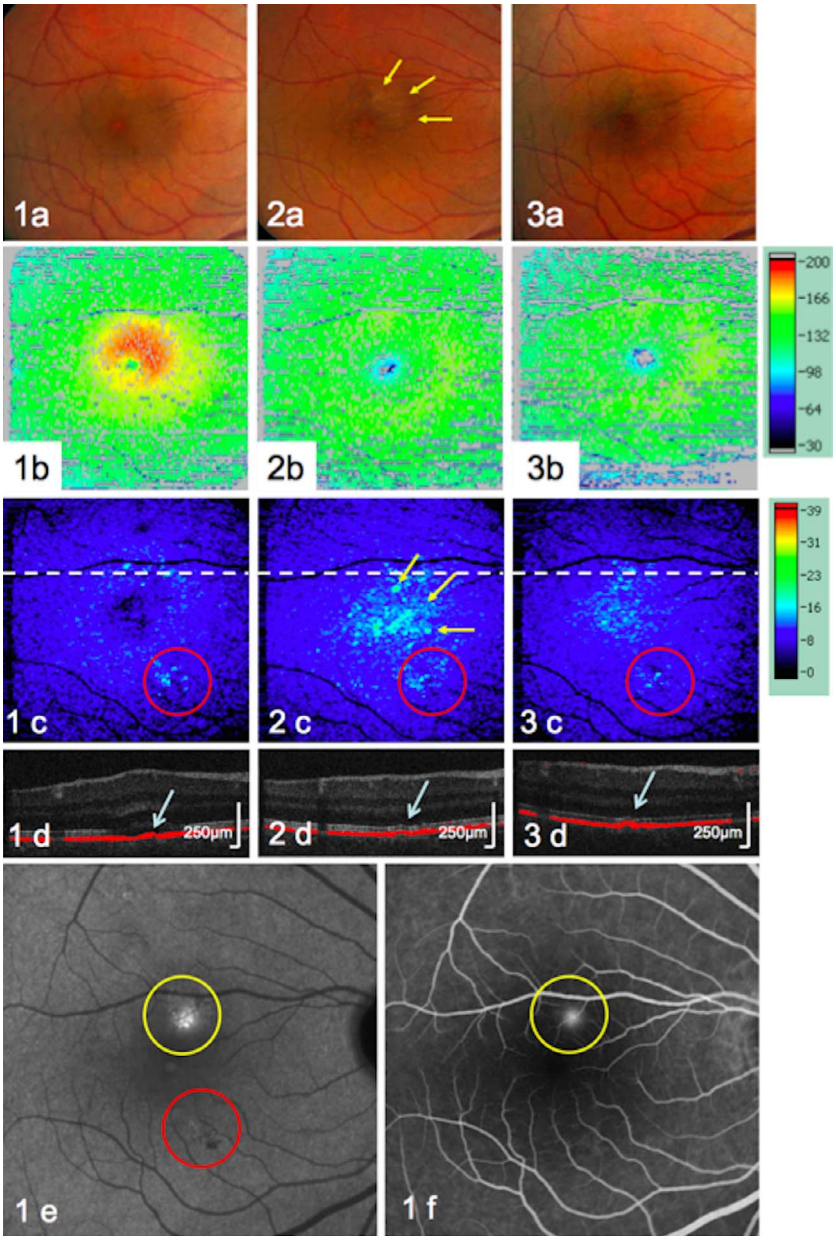

Figure 2. Right eye of a patient (male, age 34 years) with recurrent CSC. Color fundus photographs (**1a–3a**); PS-OCT retinal thickness maps (**1b–3b**); PS-OCT RPE maps (**1c–3c**), corresponding PS-OCT RPE segmentation B-scans ([**1d–3d**]; corresponding to *dashed white line* in PS-OCT RPE maps); late-phase ICGA (**1e**) and late-phase FA images (**1f**) at baseline (**1a–f**), 3 months (**2a–d**), and 6 months (**3a–d**). *Color bars* indicate tissue thickness in pixels. The origin of dye leakage was a small, flat PED superior to the fovea and can be located in FA and ICGA images from the baseline visit (*yellow circle* in [**1e**], [**1f**]; *white arrows* in [**1–3d**]). Inferior to the fovea, RPE aggregations were visible in PS-OCT (*red circles*), corresponding to a hypocyanescent area in ICGA (**1e**), but were not visible on fundus examination. In and around the fovea, RPE aggregations were abundant after resolution of SRF (*yellow arrows* in [**2a**, **2c**]) and were clearly visualized by PS-OCT, but hardly visible by CF images. The pigment epithelium detachment did not change significantly in size (*white arrow* in [**2d**]). At 6 months, the RPE aggregations were considerably reduced yet still visible on PS-OCT.

Figures 2 through 4 illustrate examples of RPE anomalies imaged by PS-OCT in eyes with CSC from our dataset.

Qualitative PS-OCT Findings

For frequencies of the evaluated PS-OCT parameters, see Tables 2 and 3.

In 10 study eyes and one fellow eye, a reliable evaluation of RPE skip lesions, RPE thickening and RPE atrophy was not possible in PS-OCT at baseline due to the amounts of SRF, which obscured the signal originating from the RPE (see Table 2). However, after resolution of SRF, a detailed analysis was carried out in all eyes.

Interestingly, RPE features observed in the fellow eyes corresponded well with pathologic angiographic features (e.g., staining, hypofluorescence), indicative of previous (subclinical) episodes of CSC. Only one of a total of nine fellow eyes with RPE changes showed no anomalies on angiography despite the presence of RPE skip lesions and small RPE aggregations on PS-OCT imaging.

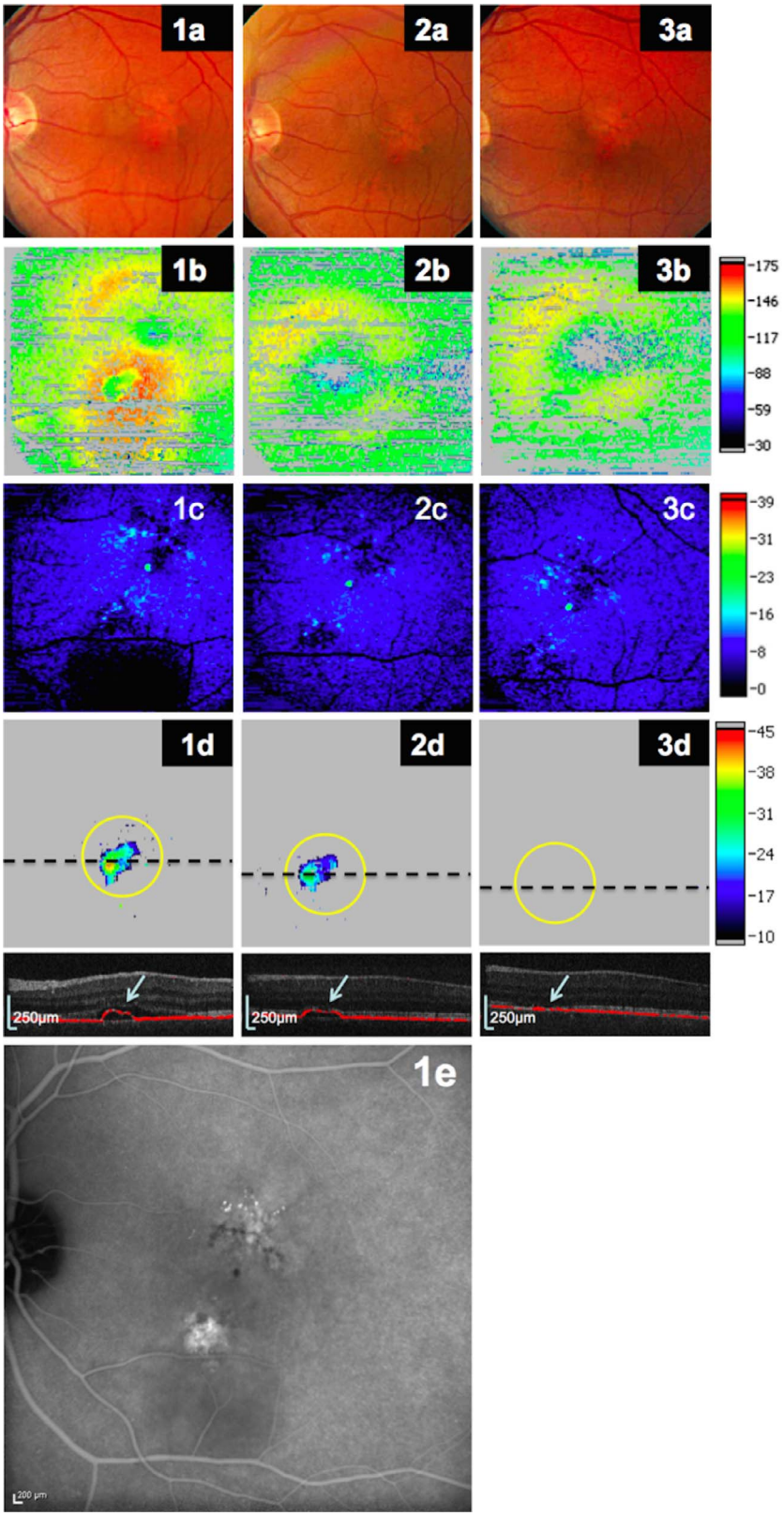

Figure 3. Left eye of a patient (male, age 40 years) with recurrent CSC. Color fundus photographs (**1a–3a**); PS-OCT retinal thickness maps (**1b–3b**) PS-OCT RPE maps (**1c–3c**); PS-OCT PED maps and PS-OCT RPE segmentation B-scans (corresponding to *dashed line*, [**1d–3d**]); and late-phase ICGA (**1e**) at baseline (**1a–d**, **1e**), after 4.5 months (resolved SRF; [**2a–d**]) and after 8 months (**3a–d**). *Color bars* indicate tissue thickness in pixels. After resolution of SRF, the PED (*yellow circle*) decreased in size by 24% in volume and by 8% in area (**2d**) by month 4.5. At a re-evaluation visit at month 8, the patient presented with a complete resolution of the PED (**3a–d**).

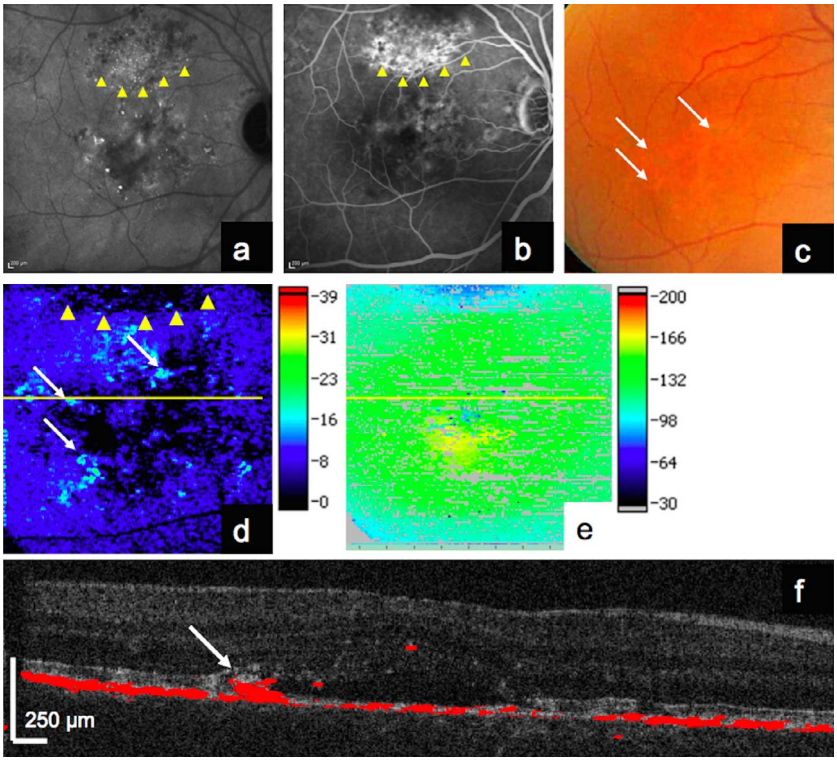

FIGURE 4. Right eye of a patient (male, age 44 years) with recurrent CSC. Late-phase ICGA (**a**), late-phase FA (**b**), CF (**c**), PS-OCT RPE thickness map (**d**), PS-OCT retinal thickness map (**e**) and PS-OCT RPE segmentation B-scan (**f**). The *yellow lines* in (**d**) and (**e**) indicate the location of the corresponding B-scan; *color bars* indicate tissue thickness in pixels. Patches of RPE atrophy (*yellow arrowheads*) and RPE thickening (*white arrows*) can be identified in the PS-OCT RPE thickness map (**d**) and B-scan (**f**) corresponding well to areas of irregular staining and dye leakage in ICGA and FA (**a**, **b**). Presence and extent of respective RPE abnormalities are barely visible on CF (**c**).

Closure of RPE Microrips (Leakage Sites)

After resolution of fluid, the RPE appeared continuous at the former leakage site in eight (32%) eyes. In five (20%) of these eyes, RPE hypertrophy was present at that specific location; in the other three eyes (12%), normal RPE thickness was observed. In the remaining 17 (68%) eyes, 2 (8%) developed an RPE atrophy and in 15 (60%) eyes, skip lesions were observed at the former leakage spot (Fig. 5). However, the RPE changes observed after resolution of SRF were more widespread and not limited to the location of leakage in FA or ICGA.

DISCUSSION

In this observational study, a novel tissue-contrast sensitive imaging modality, PS-OCT, was used to identify clinically visible as well as subclinical RPE alterations in the course of an episode of active CSC. Findings were compared with current imaging standards such as SD-OCT, ICGA, FA, and CF.

Eleven participants were diagnosed with recurrent CSC based on ICGA and FA. However, only one of the patients had been diagnosed with CSC prior to study inclusion. Extrafoveal

TABLE 2. RPE Characteristics on PS-OCT in Eyes With CSC

	Baseline		End of Study	
	Study Eyes, $n = 25$	**Fellow Eyes, $n = 23$**	**Study Eyes, $n = 25$**	**Fellow Eyes, $n = 23$**
RPE aggregations, *n* (%)				
Present	25 (100)	6 (26)	25 (100)	6 (26)
Evaluation not possible	0 (0)	0 (0)	0 (0)	0 (0)
RPE skip lesions, *n* (%)				
Present	15 (60)	7 (30)	23 (92)	7 (30)
Evaluation not possible	10 (40)	0 (0)	0 (0)	0 (0)
RPE thickening, *n* (%)				
Present	8 (32)	2 (9)	11 (44)	2 (9)
Evaluation not possible	10 (40)	0 (0)	0 (0)	0 (0)
RPE atrophy, *n* (%)				
Present	2 (8)	2 (9)	3 (12)	2 (9)
Evaluation not possible	10 (40)	1 (4)	0 (0)	0 (0)

PS-OCT findings in study eyes and fellow eyes at baseline (active CSC) and after resolution of SRF (resolved CSC).

Table 3. RPE Characteristics on PS-OCT in Study Eyes With Acute CSC and Recurrent CSC

	Baseline		End of Study	
	Acute, $n = 14$	Recurrent, $n = 11$	Acute, $n = 14$	Recurrent, $n = 11$
RPE aggregations, *n* (%)				
Present	14 (100)	11 (100)	14 (100)	11 (100)
Evaluation not possible	0 (0)	0 (0)	0 (0)	0 (0)
RPE skip lesions, *n* (%)				
Present	6 (43)	9 (82)	13 (93)	10 (91)
Evaluation not possible	8 (57)	2 (18)	0 (0)	0 (0)
RPE thickening, *n* (%)				
Present	3 (21)	5 (45)	5 (36)	6 (55)
Evaluation not possible	6 (43)	4 (36)	0 (0)	0 (0)
RPE atrophy, *n* (%)				
Present	0 (0)	2 (18)	0 (0)	3 (27)
Evaluation not possible	5 (36)	5 (45)	0 (0)	0 (0)

PS-OCT findings in eyes with acute versus eyes with recurrent CSC at baseline and after resolution of SRF.

lesions that do not cause foveal neuroretinal detachment tend to be asymptomatic, particularly, when the fellow eye has good visual function and compensates for the affected eye.[1] The pathologic findings in ICGA/FA and PS-OCT indicate that many of the pathologic processes in CSC go by unnoticed by the patient, albeit not without damage to the RPE.

Area and volume of PEDs were relatively stable at presentation of active CSC and after resolution of SRF in our study population. A nonsignificant tendency toward a decrease (rather than an increase) in size was seen in several cases accompanied by a spontaneous resolution of SRF. Therefore, a further decrease or even full resolution of PEDs at a later point in time seems likely, however, could not consistently be observed in this short-term follow-up study. The reason why certain PEDs were subject to shrinkage while other PEDs remained stable in size remains elusive. In a recent article by Song and colleagues,[14] no statistically significant difference was observed in PED morphology as seen on SD-OCT between different stages of CSC (acute, chronic, or early chronic CSC), which is in agreement with the observations in our study. Fujimoto and colleagues[13] presented a case series involving 21 eyes with CSC showing that only 5 out of 14 PEDs with leakage

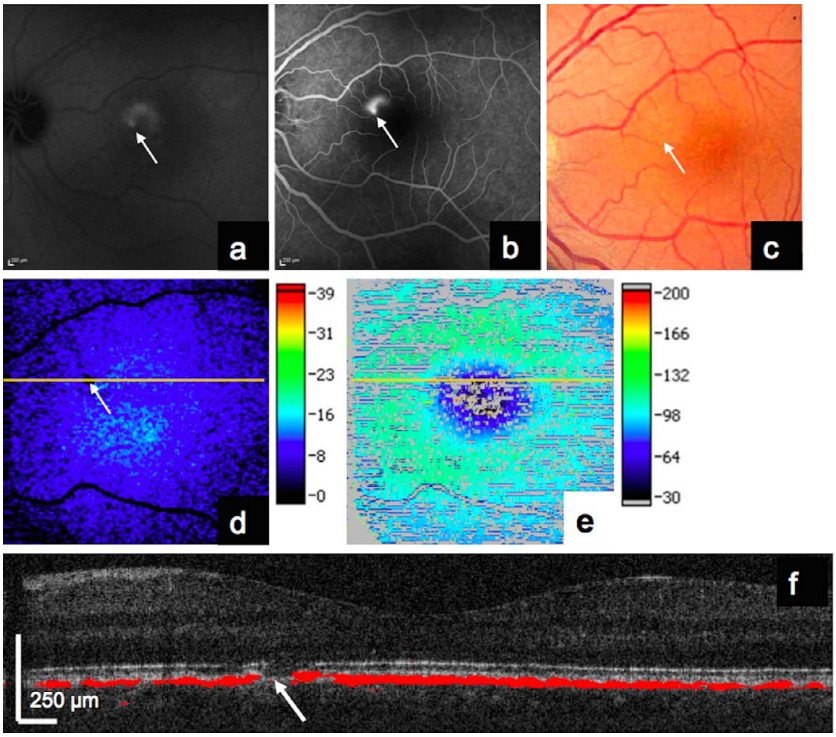

Figure 5. Left eye of a patient (male, age 43 years) with acute CSC. Late-phase ICGA (**a**), late-phase FA (**b**), CF (**c**) at baseline; PS-OCT RPE thickness map (**d**), PS-OCT retinal thickness map (**e**) and PS-OCT RPE segmentation B-scan (**f**) 5 months after resolution of SRF. The *yellow lines* in (**d**) and (**e**) indicate the location of the corresponding B-scan; *color bars* indicate tissue thickness in pixels. Notice the "smokestack" pattern of dye leakage of a single microrip in (**a**) and (**b**). Five months after resolution of acute CSC, a disruption of the RPE corresponding to the origin of leakage can still be identified on PS-OCT (*white arrow*, [**d**, **f**]).

at baseline persisted after resolution of SRF. However, in contrast to the study described herein, thermal laser was applied in the majority of the study eyes.[13]

In our study, RPE aggregations as seen on PS-OCT were noted in all study eyes after resolution of SRF; however, in some cases the aggregations started to resolve and were barely detectable 3 months after resolution of SRF. In eyes diagnosed with recurrent CSC, RPE aggregations corresponded well to areas of hypocyanescence in ICGA, likely caused by previous episodes of CSC. It is further likely that these RPE abnormalities do not involute completely and that even asymptomatic episodes of CSC might leave behind RPE anomalies detectable by PS-OCT (Figs. 2, 3, 5).

Skip lesions of RPE or blowouts were observed in PS-OCT en-face maps of 15 study eyes in the acute CSC episode. In the remaining 10 study eyes, however, an exact evaluation was not possible due to a shadowing effect caused by profound accumulations of SRF. Skip lesions of RPE were present in 23 eyes (92%) after resolution of SRF. Skip lesions of RPE were scattered across the corresponding area of serous neuroretinal detachment and did not exclusively correspond to the site of leakage or staining in angiography. Using en-face SD-OCT, van Velthoven and coworkers[12] also found widespread RPE anomalies in CSC, such as small PEDs, suggesting that the RPE might be affected diffusely rather than only localized.

Using en-face OCT, RPE features like microrips or PED associated with CSC have been described previously.[10–12] However, on intensity-based en-face imaging, RPE identification is dependent on the correct C-scan position within the three-dimensional SD-OCT cube and different layers of the retina are hard to differentiate in eyes with retinal pathology. In contrast, using PS-OCT, the RPE is segmented based on its physical property to depolarize light; hence, a differentiation from tissues with similar reflectivity is possible even in eyes with retinal pathology. In a recent publication, Gupta and colleagues[10] observed a spontaneous closure of RPE microrips accompanied by the resolution of SRF. In the study described herein, such closure of RPE microrips was not consistently observed in all eyes. The retinal pigment epithelium appeared to be continuous at the former leakage site in eight (32%) eyes and in five (20%) of these eyes, RPE thickening was observed at that specific location. In the remaining 17 (68%) eyes, discontinuities of the RPE were still present at the former leakage site even after resolution of SRF (Fig. 5). Fifteen (60%) of these eyes showed RPE skip lesions and two (8%) eyes RPE atrophy at the former leakage area. These findings may support the hypothesis of a rebalance of choroidal perfusion pressure gradients, as hypothesized by Caccavale et al.,[27] rather than a closure of the defect by RPE migration and hyperplasia. Whether eyes with persistent RPE defects have a higher risk of recurrence still has to be evaluated in a longer follow up.

Using PS-OCT, a detailed evaluation of the RPE integrity was feasible in all eyes once SRF had resolved. Even very subtle changes of the RPE, which in many cases were barely visible on SD-OCT or clinical examination (Fig. 5), were identified using PS-OCT. The ability to detect even subclinical morphologic changes is of clinical importance as these might suggest previous episodes of CSC, leading the clinician to a more frequent follow up of these patients. Earlier detection of CSC episodes facilitates earlier therapeutic intervention, especially in eyes with recurrent CSC. Eyes with recurrent CSC are at a higher risk of vision loss and development of secondary CNV, a severely vision threatening neovascular disease that requires further invasive intravitreal treatment.[5,28] Together with conventional FA and ICGA imaging, PS-OCT may improve the risk assessment of CNV membrane formation in patients with recurrent CSC by detection of subclinical RPE changes indicative of recurrent or chronic episodes of CSC.

The authors are aware of certain limitations of this study. Only a relatively small number of eyes were included in the study, as the inclusion criteria were restrictive and reliable imaging was hampered in some cases due to fixation loss during the acute episode of CSC, causing imaging motion artifacts. As only the natural course of RPE changes during the disease should be investigated in this study, eyes that received treatment (i.e., reduced-fluence PDT) were excluded from the study. Only the macula was investigated, so changes of the RPE outside the field of view of the PS-OCT instrument (6.2×6.7 mm; X × Y) might have been missed. However, the PS-OCT scans were centered on the fovea to ensure that the same retinal area was covered during follow-up.

In conclusion, this study demonstrates that PS-OCT is capable of detecting even very subtle RPE changes in eyes with CSC that might not be visible on clinical examination. PED, automatically identified by PS-OCT, did not significantly change in size in the short-term follow-up. Closure of RPE at the leakage site was observed in about one-third of all study eyes, suggesting that further mechanisms are involved in recovery of CSC.

The detection of such subclinical lesions might serve as an indicator of previous (subclinical) episodes of CSC, which might necessitate more individualized follow-up regimen.

Acknowledgments

Supported by the Austrian Science Fund (imaging device development; FWF grant P19624-B02). The authors alone are responsible for the content and writing of the paper.

Disclosure: **P. Roberts**, Canon Inc. (F); **B. Baumann**, Canon Inc. (F); **J. Lammer**, None; **B. Gerendas**, None; **J. Kroisamer**, None; **W. Bühl**, None; **M. Pircher**, Canon Inc. (F); **C.K. Hitzenberger**, Canon Inc. (F); **U. Schmidt-Erfurth**, Alcon Laboratories, Inc. (C), Allergan (C), Bayer Healthcare (C), Boehringer (C), Novartis (C); **S. Sacu**, None

References

1. Wang M, Munch IC, Hasler PW, Prünte C, Larsen M. Central serous chorioretinopathy. *Acta Ophthalmologica*. 2008;86:126–145.
2. Gilbert CM, Owens SL, Smith PD, Fine SL. Long-term follow-up of central serous chorioretinopathy. *Br J Ophthalmol*. 1984;68:815–820.
3. Spaide RF, Campeas L, Haas A, et al. Central serous chorioretinopathy in younger and older adults. *Ophthalmology*. 1996;103:2070–2080.
4. Karim SP, Adelman RA. Profile of verteporfin and its potential for the treatment of central serous chorioretinopathy. *Clin Ophthalmol*. 2013;7:1867–1875.
5. Nicholson B, Noble J, Forooghian F, Meyerle C. Central serous chorioretinopathy: update on pathophysiology and treatment. *Surv Ophthalmol*. 2013;58:103–126.
6. Yannuzzi LA. Central serous chorioretinopathy: a personal perspective. *Am J Ophthalmol*. 2010;149:361–363.
7. Tittl MK, Spaide RF, Wong D, et al. Systemic findings associated with central serous chorioretinopathy. *Am J Ophthalmol*. 1999;128:63–68.
8. Ross A, Ross AH, Mohamed Q. Review and update of central serous chorioretinopathy. *Curr Opin Ophthalmol*. 2011;22:166–173.
9. Gupta P, Gupta V, Dogra MR, Singh R, Gupta A. Morphological changes in the retinal pigment epithelium on spectral-domain OCT in the unaffected eyes with idiopathic central serous chorioretinopathy. *Int Ophthalmol*. 2010;30:175–181.

10. Gupta V, Gupta P, Dogra MR, Gupta A. Spontaneous closure of retinal pigment epithelium microrip in the natural course of central serous chorioretinopathy. *Eye (Lond)*. 2010;24:595–599.
11. Hirami Y, Tsujikawa A, Gotoh N, Iwama D, Yoshimura N. Alterations of retinal pigment epithelium in central serous chorioretinopathy treated by laser photocoagulation. *Jpn Ophthalmol*. 2007;51:477–478.
12. van Velthoven ME, Verbraak FD, Garcia PM, Schlingemann RO, Rosen RB, de Smet MD. Evaluation of central serous retinopathy with en face optical coherence tomography. *Br J Ophthalmol*. 2005;89:1483–1488.
13. Fujimoto H, Gomi F, Wakabayashi T, Sawa M, Tsujikawa M, Tano Y. Morphologic changes in acute central serous chorioretinopathy evaluated by Fourier-domain optical coherence tomography. *Ophthalmology*. 2008;115:1494–1500, 1500.e1–2.
14. Song IS, Shin YU, Lee BR. Time-periodic characteristics in the morphology of idiopathic central serous chorioretinopathy evaluated by volume scan using spectral-domain optical coherence tomography. *Am J Ophthalmol*. 2012;154:366–375.e4.
15. Shin YU, Lee BR. Retro-mode Imaging for retinal pigment epithelium alterations in central serous chorioretinopathy. *Am J Ophthalmol*. 2012;154:155–163. e4.
16. Dansingani KK, Balaratnasingam C, Naysan J, Freund KB. En face imaging of pachychoroid spectrum disorders with swept-source optical coherence tomography. *Retina*. 2016;36:499–516.
17. Pircher M, Götzinger E, Findl O, et al. Human macula investigated in vivo with polarization-sensitive optical coherence tomography. *Invest Ophthalmol Vis Sci*. 2006;47:5487–5494.
18. Pircher M, Hitzenberger CK, Schmidt-Erfurth U. Polarization sensitive optical coherence tomography in the human eye. *Prog Retin Eye Res*. 2011;30:431–451.
19. Baumann B, Baumann SO, Konegger T, et al. Polarization sensitive optical coherence tomography of melanin provides intrinsic contrast based on depolarization. *Biomed Opt Express*. 2012;3:1670–1683.
20. Baumann B, Götzinger E, Pircher M, Hitzenberger CK. Measurements of depolarization distribution in the healthy human macula by polarization sensitive OCT. *J Biophotonics*. 2009;2:426–434.
21. Baumann B, Gotzinger E, Pircher M, et al. Segmentation and quantification of retinal lesions in age-related macular degeneration using polarization-sensitive optical coherence tomography. *J Biomed Opt*. 2010;15:061704.
22. Götzinger E, Pircher M, Geitzenauer W, et al. Retinal pigment epithelium segmentation by polarization sensitive optical coherence tomography. *Optics express*. 2008;16:16410–16422.
23. Schütze C, Ahlers C, Pircher M, et al. Morphologic characteristics of idiopathic juxtafoveal telangiectasia using spectral-domain and polarization-sensitive optical coherence tomography. *Retina*. 2012;32:256–264.
24. Schlanitz FG, Baumann B, Spalek T, et al. Performance of automated drusen detection by polarization-sensitive optical coherence tomography. *Invest Ophthalmol Vis Sci*. 2011;52:4571–4579.
25. Baraki H, Feltgen N, Roider J, Hoerauf H, Klatt C. Central serous chorioretinopathy (CSC) [in German]. *Ophthalmologe*. 2010;107:479–492. quiz 493.
26. Quin G, Liew G, Ho IV, Gillies M, Fraser-Bell S. Diagnosis and interventions for central serous chorioretinopathy: review and update. *Clin Experiment Ophthalmol*. 2013;41:187–200.
27. Caccavale A, Romanazzi F, Imparato M, Negri A, Morano A, Ferentini F. Central serous chorioretinopathy: a pathogenetic model. *Clin Ophthalmol*. 2011;5:239–243.
28. Loo RH, Scott IU, Flynn HW Jr, et al. Factors associated with reduced visual acuity during long-term follow-up of patients with idiopathic central serous chorioretinopathy. *Retina*. 2002;22:19–24.

Investigative Ophthalmology & Visual Science